DØ Note xxxx

A Study of Computational Algorithms for Track Fitting in the DØ Silicon Track Trigger

J. Egdemir, J. D. Hobbs, T. Mentes, W .Taylor

June 10, 1999

Abstract

Large hit multiplicities in the roads input to the level two silicon track trigger imply that in addition to track fitting, hit filtering must be performed. A variety of Hit–filtering and track–fitting algorithms for the DØ level two silicon trigger are discussed here. All are based on a linearized χ^2 fit of silicon and fiber tracker hits to a circular trajectory. The algorithms differ in the method by which the track/hit correspondance is determined given the list of silicon detector hits within a track road. Results for physics performance and algorithm processing times are presented for events which pass level one triggers similar to those expected to feed the level two silicon track trigger.

The track reconstruction phase of the run II silicon track trigger preprocessor(L2STT) uses as inputs a pair of level one central track trigger(CTT) hits and all silicon microstrip(SMT) hits within a road defined by the pair of CTT hits and the interaction point[1]. This information is used to estimate the three parameters which define a track in the $r\phi$ plane: the impact parameter b, the track direction at the point of closest approach ϕ_0 and the track curvature κ. There are two parts to this task: (1) determining which of the hits in a given CTT road belong on the track and (2) determining the track parameters. In practice, the order and separability of these two steps depends critically on the algorithm being used. Initial studies are described elsewhere[2]. This note contains results from testing the physics performance and execution time for four different algorithms on a variety of processors.

This note has four sections. The first is a description of the track parameter definitions and approximations made in determining the trajectory. The second describes the simulated data samples used in this study, and the third describes the various hit filtering options and contains physics performance results. The fourth section contains the timing results.

1 Track Parameters

A track in the $r\phi$ plane can be defined by the following three parameters:

- b, the distance between the track and the origin at the point on the track closest to the origin[1],
- ϕ_0, the track direction at this point and
- $|\kappa| \equiv 1/(2R)$ the track curvature at the same point.

Here R is the radius of curvature of the track at the point of closest approach. The sign of κ is the negative of the particle charge, and the impact parameter is signed such that the product $b\kappa$ is negative if the origin is inside the circle defining the trajectory and is positive if the origin is outside the circle defining the trajectory.

In the absence of interactions with material, the trajectory of a charged particle in the $r\phi$ plane is circular. The equation describing this trajectory is

$$r\kappa(1 - 2b\kappa)\sin(\phi - \phi_0) = (r\kappa)^2 + b\kappa(1 - b\kappa). \tag{1}$$

Here (r, ϕ) is a point on the track expressed in cylindrical coordinates. The parameters b, κ and ϕ_0 are typically found by minimizing a χ^2 based on the differences between the trajectory and the associated (r, ϕ) points. If the particle interacts with matter, then the direction will change at the point of the interaction, giving a kink in the trajectory. This is typically incorporated into a χ^2 by adding terms which express the track parameters of the trajectory after the scatter in terms of the parameters before the scatter, the unknown scattering angle $\delta\phi$ and the RMS scattering angle α. The scattering angle $\delta\phi$ appears as an additional parameter in the track fit.

To reduce the algebraic complexity of the equation for the track trajectory, the following are assumed for the L2STT:

- there is no energy loss or multiple scattering from interactions in the beam pipe or the tracking detectors, and
- $b\kappa \ll 1$, $r\kappa \ll 1$ and $\phi - \phi_0 \ll 1$ for a silicon hit at the position (r, ϕ).

The first of these requirements implies that the trajectory remains circular in the transverse plane. The second allows us to use a small parameter expansion for equation 1. For DØ, the largest impact parameter is $b \approx 2$ mm, the largest hit radius is $r \approx 50$ cm and the largest curvature is $\kappa \approx 0.002$ cm^{-1}. Thus $b\kappa < 0.004$ and $r\kappa < 0.1$. For a track with $b \approx 2$ mm and $\kappa \approx 0.002$ cm^{-1} and a hit at the smallest SMT radius $r \approx 3$ cm, $\phi - \phi_0 < 0.07$.

Under these assumptions, only leading terms in the product $b\kappa$ and $r\kappa$ are retained, and $\sin(\phi - \phi_0) \approx \phi - \phi_0$. Equation 1 then becomes

$$\phi(r) = b/r + \kappa r + \phi_0. \tag{2}$$

[1] This distance is called the impact parameter

The best estimate of the three track parameters is found by minimizing the χ^2 given by

$$\chi^2 = \sum_{i=hits} \left[\frac{\phi_i - (b/r_i + \kappa r_i + \phi_0)}{\sigma_{\phi i}} \right]^2 \tag{3}$$

$$= \sum_{i=hits} \left[\frac{r_i\phi_i - (b + \kappa r_i^2 + r_i\phi_0)}{\sigma_i} \right]^2 . \tag{4}$$

in which all SMT and CFT hits associated with the track are used. Here $\sigma_{\phi i}$ is the ϕ measurement error on a hit at (r_i, ϕ_i) and $\sigma_i \equiv r_i\sigma_{\phi i}$ is the measurement error expressed in the $r\phi$ plane. For the case of L2STT, the set of hits consists of at most one hit per SMT layer and two CFT hits. Because the χ^2 is quadratic in the track parameters, the minimization can be performed analytically, resulting in the following system of equations for the fit parameters:

$$\begin{pmatrix} b \\ \kappa \\ \phi_0 \end{pmatrix} = \begin{pmatrix} \sum 1/\sigma_i^2 & \sum r_i^2/\sigma_i^2 & \sum r_i^1/\sigma_i^2 \\ \sum r_i^2/\sigma_i^2 & \sum r_i^4/\sigma_i^2 & \sum r_i^3/\sigma_i^2 \\ \sum r_i^1/\sigma_i^2 & \sum r_i^3/\sigma_i^2 & \sum r_i^2/\sigma_i^2 \end{pmatrix}^{-1} \begin{pmatrix} \sum \phi_i r_i^1/\sigma_i^2 \\ \sum \phi_i r_i^3/\sigma_i^2 \\ \sum \phi_i r_i^2/\sigma_i^2 \end{pmatrix}$$

2 Data Samples

Six simulated data samples are used in this study. The first is a sample of single muon events with p_T's of 3, 5, 10 and 15 GeV. The second and third are $Z \to b\bar{b}$ samples with zero or two additional minbias interactions. The fourth and fifth are $WH \to q\bar{q'}b\bar{b}$ events, again with zero or two additional minbias interactions. The final sample is a background sample formed by a composite of QCD samples[3] generated to simulate the track and jet multiplicity of minimum bias events.

The samples were generated with the full upgrade geant program using the Feb. '97 release.[2] Further processing and trigger rate determination were done using the standard ntuple–based trigger simulation and the PAC '98 trigger menu[4].

Figures 1 through 4 show the distributions of the layer with the highest multiplicity, the multiplicity of that layer, the number of CTT roads per event, the number of CTT roads per SMT sector[3] and the maximum number of CTT roads per sector per event for the $Z \to b\bar{b}$ and $WH \to q\bar{q'}b\bar{b}$ samples. The events were required to pass level one triggers similar to those expected to feed the L2STT. For similar plots without any trigger applied, see[5].

3 Hit Filtering Algorithms

In order to obtain the best possible performance, it is important to select the hits that arise from each charged particle. detector. If there is more than one hit per silicon layer in a road, the "correct" hit must be determined. The number of hits per layer per road depends

[2] The single muon samples were generated using the Aug '96 release.

[3] The SMT is divided into six 60° sectors with an extra $\pm 9^o$ of fiber tracker coverage feeding into a given SMT sector. The extra fiber tracker coverage accounts for the tracks which curve out of the initial 60° wedge defined by the silicon sector as they go through the fiber tracker.

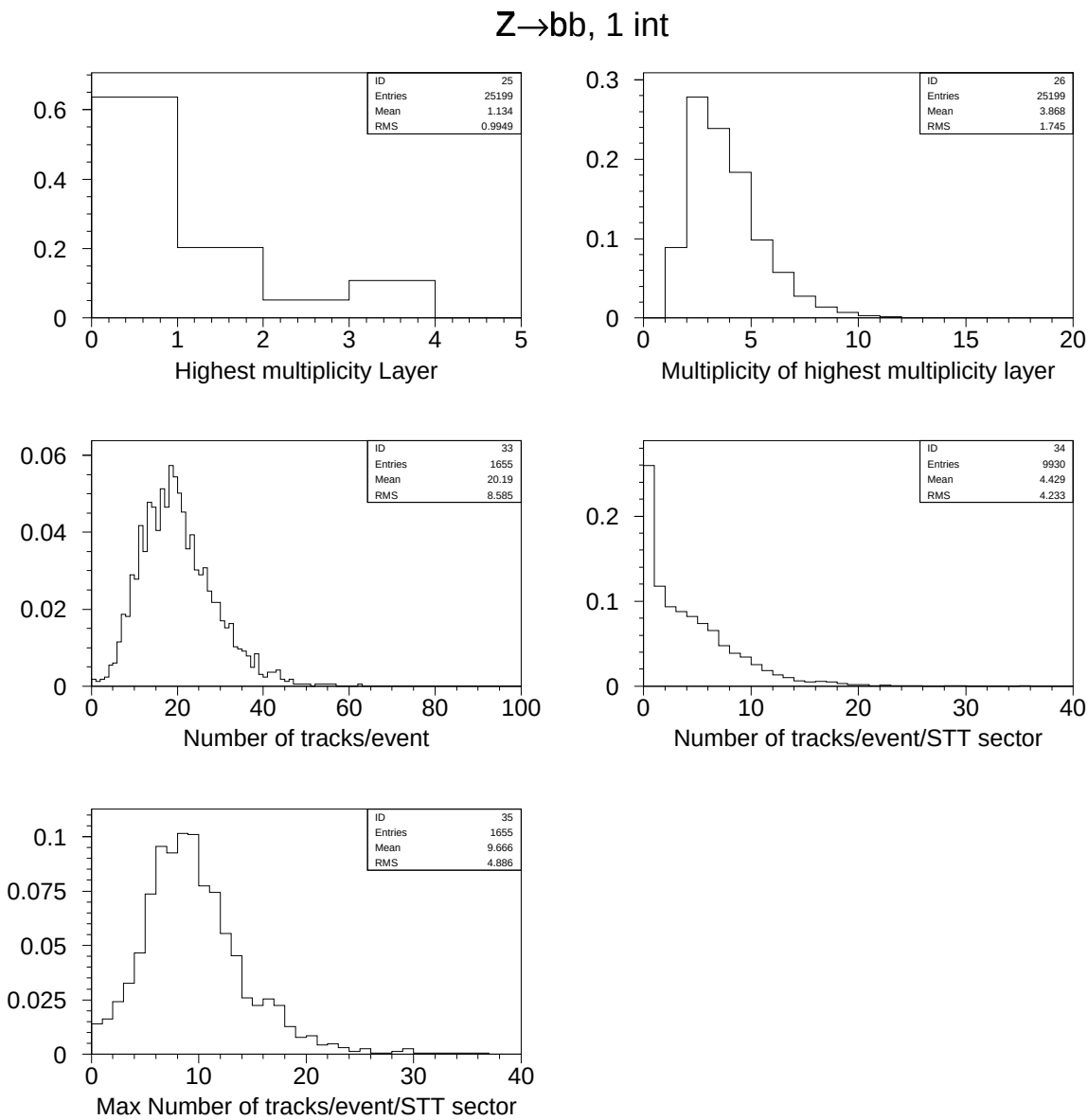

Figure 1: The distributions of layer with highest multiplicity, the multiplicity of that layer (upper right), the number of CTT roads per event (middle left), the number of CTT roads per sector per event (middle right) and the maximum number of CTT roads per sector per event (lower left). The sample is the $Z \rightarrow b\bar{b}$(1 interaction) sample, and the event were required to pass triggers similar to those expected to feed the L2STT.

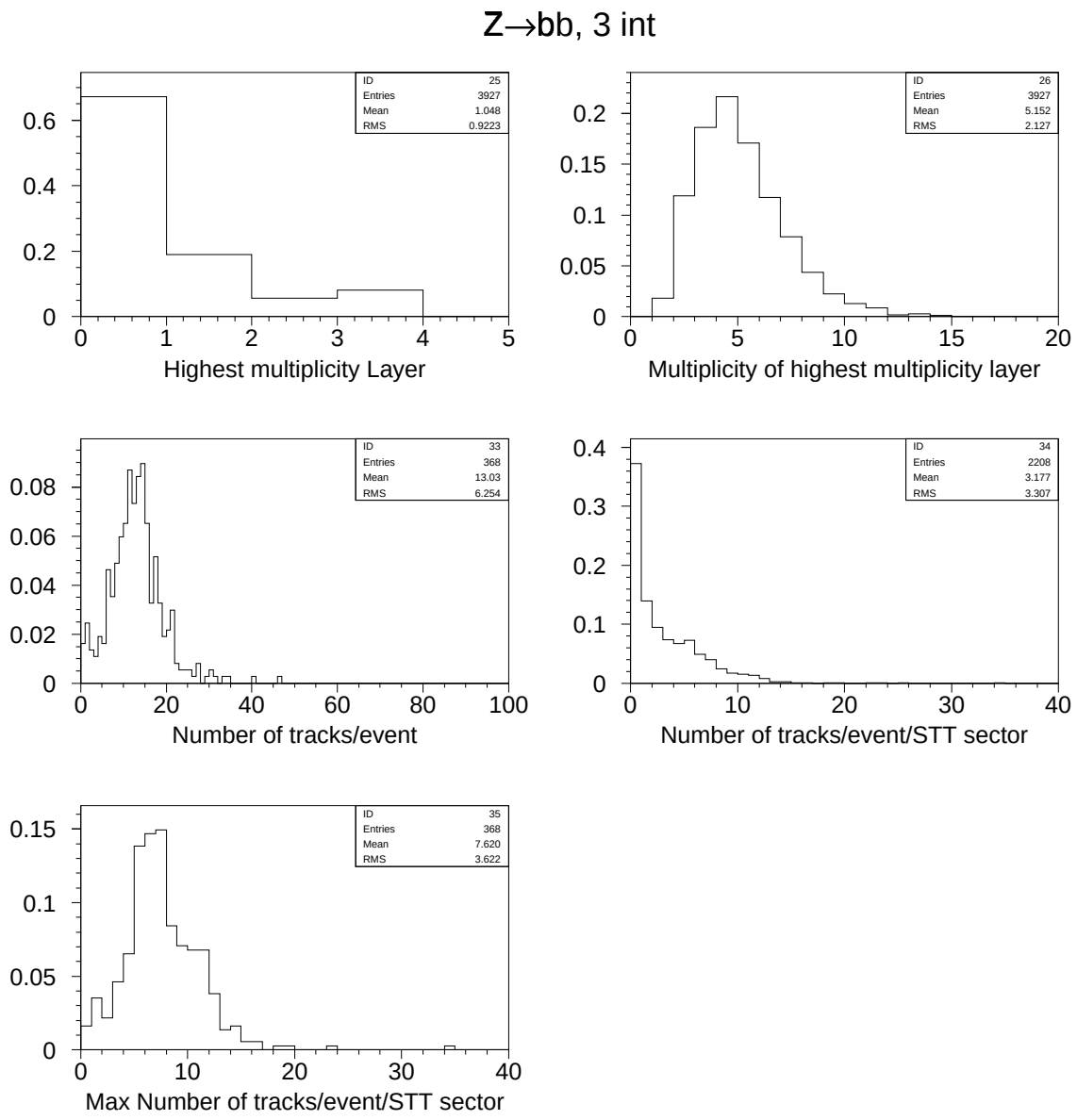

Figure 2: The distributions of layer with highest multiplicity, the multiplicity of that layer (upper right), the number of CTT roads per event (middle left), the number of CTT roads per sector per event (middle right) and the maximum number of CTT roads per sector per event (lower left). The sample is the $Z \rightarrow b\bar{b}$(3 interactions) sample, and the event were required to pass triggers similar to those expected to feed the L2STT.

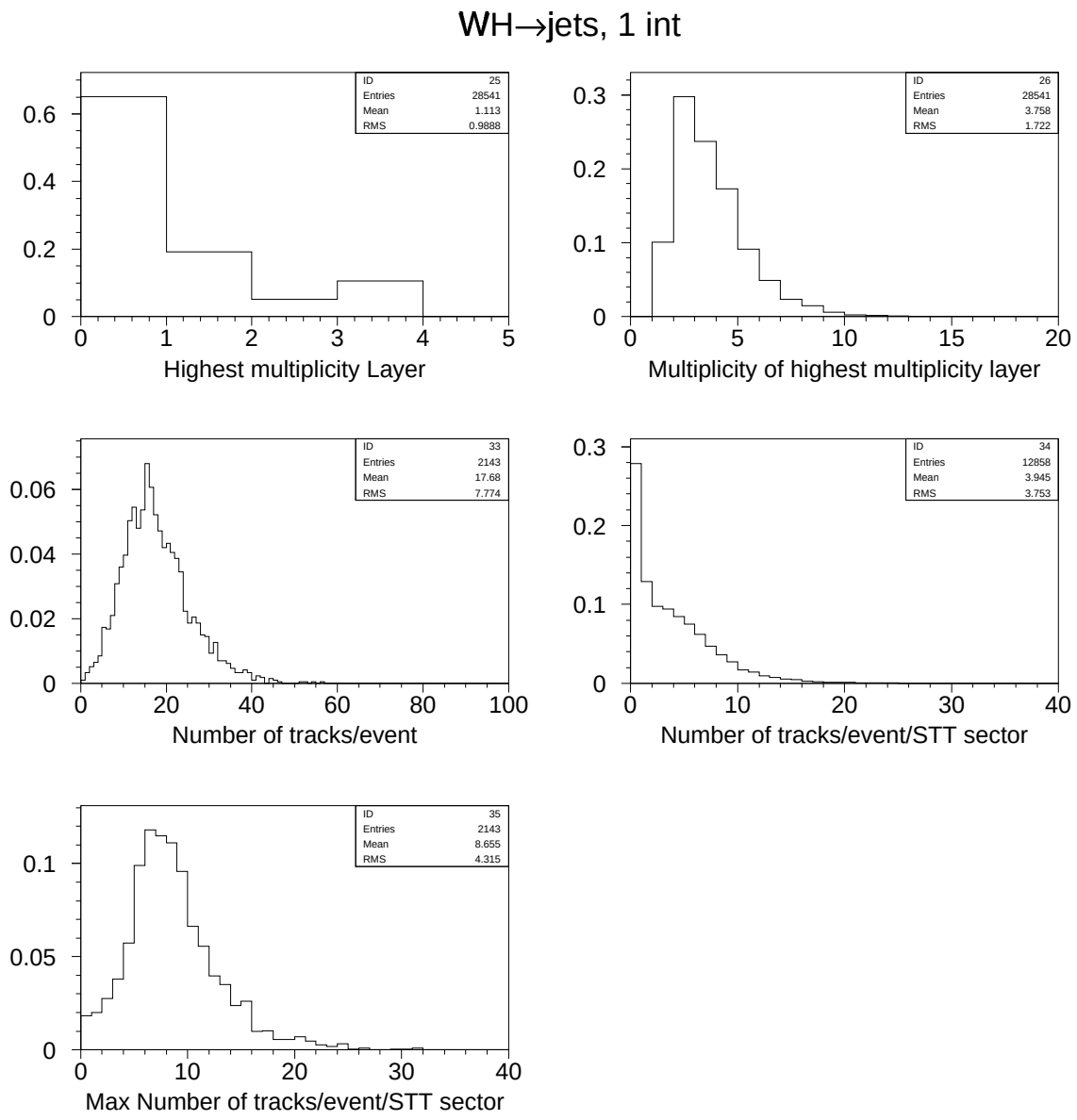

Figure 3: The distributions of layer with highest multiplicity, the multiplicity of that layer (upper right), the number of CTT roads per event (middle left), the number of CTT roads per sector per event (middle right) and the maximum number of CTT roads per sector per event (lower left). The sample is the $WH \rightarrow q\overline{q'}b\overline{b}$(1 interaction) sample, and the event were required to pass triggers similar to those expected to feed the L2STT.

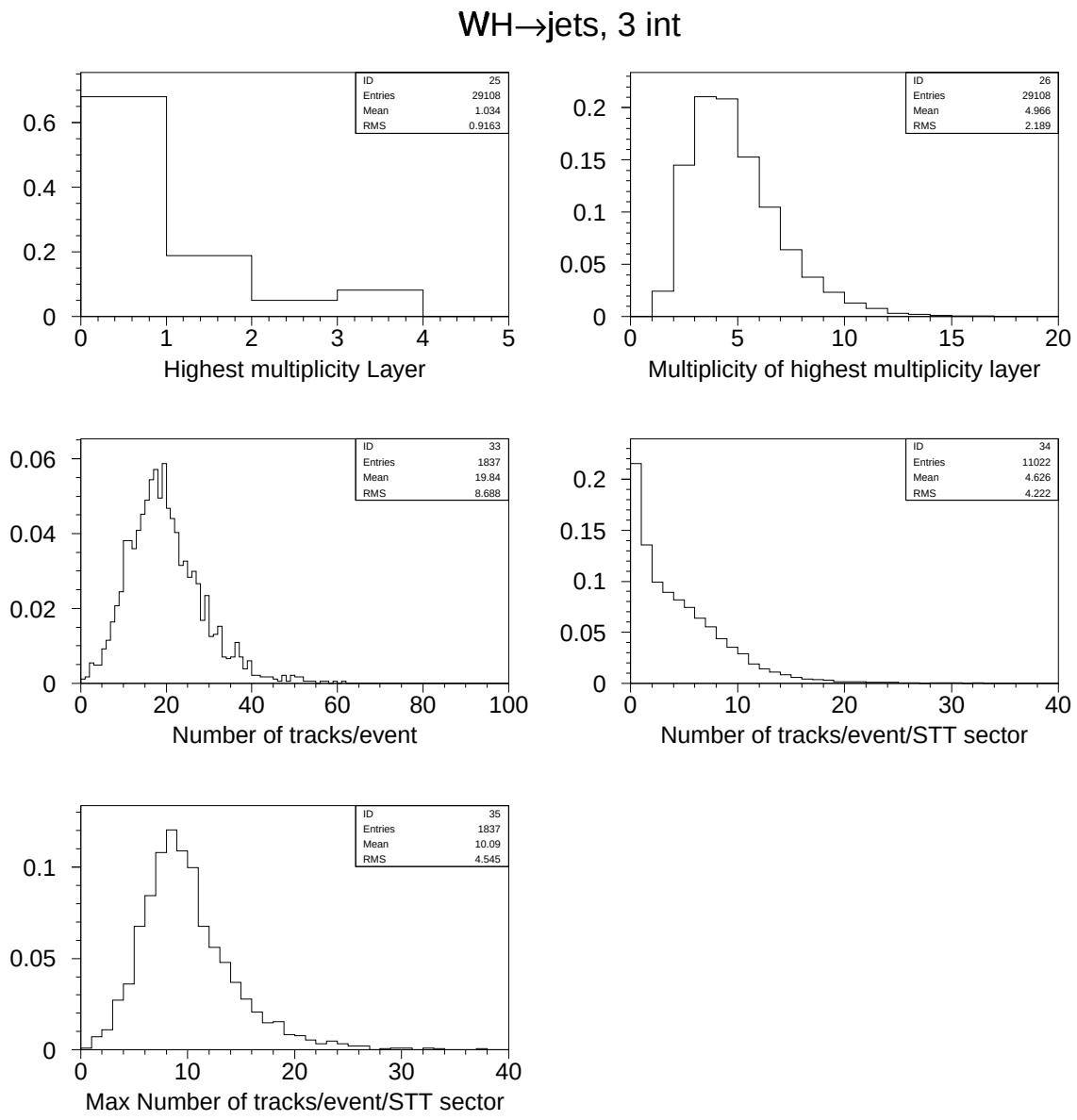

Figure 4: The distributions of layer with highest multiplicity, the multiplicity of that layer (upper right), the number of CTT roads per event (middle left), the number of CTT roads per sector per event (middle right) and the maximum number of CTT roads per sector per event (lower left). The sample is the $WH \rightarrow q\overline{q'}b\overline{b}$(3 interactions) sample, and the event were required to pass triggers similar to those expected to feed the L2STT.

Process	# of Interactions	N	F_2
Single μ	1	1.5	0.470
$Z \to b\bar{b}$	1	3.3	0.918
	3	4.5	0.982
$WH \to q\bar{q}'b\bar{b}$	1	3.2	0.894
	3	5.2	0.978
Dijet	1-7	5.2	0.982

Table 1: Hit multiplicity per road in the layer with the highest occupancy (N) and fraction of tracks with two or more hits per road in the layer with the highest occupancy (F_2) for different numbers of interactions/beam crossing. For all entries, the statistical error is negligible.

on the event topology, the luminosity and the noise in the detector. Table 1 shows the average number of hits/layer/road and the fraction of layers having two or more hits for different physical processes and luminosity conditions. Figure 5 shows the average number of hits/layer/road and the number of hit combinations[4] for the two $Z \to b\bar{b}$ samples. Given the large number of layers with multiple hits, attention must be paid to choosing hits. The following algorithms are being considered:

1. **Static Road-Center**: The hits closest to the circle defined by the two CTT hits and the interaction point are used in each layer.

2. **Dynamic Road-Center**: The hits closest to the center of the circle defined by the two CTT hits and the hits in SMT layer with the lowest occupancy are used. This algorithm requires looping over all hits in SMT layer with the lowest occupancy.

3. **All Combinations**: All combinations of hits are considered and the one with the best fit is chosen.

4. **Best Combination at Layer**: Moving from the outer SMT layer inwards the fit is performed at the current layer using the best result from performing fits on all combinations in the preceeding layer.

In all cases but the last the algorithm can be run in two forms. The first requires hits in all four silicon layers. The second requires hits in only three layers. The last algorithm is based on the *all combinations* algorithm, but the number of trial combinations is limited in a controlled manner. The "Static road center" algorithm uses only one hit/layer and thus has only one track per road. The "all combinations" algorithm has the number of candidate tracks equal to the product of the number of hits in each layer, reduced slightly by the requirement that all hits assigned to a track must be contained within two adjacent barrels.

[4]Hit combinations are always required to have consistant barrel topology. For example, a track is not allowed to have a layer one hit in barrel one, a layer two hit in barrel two and the layer three hit again in barrel one. At most one change in barrel is allowed.

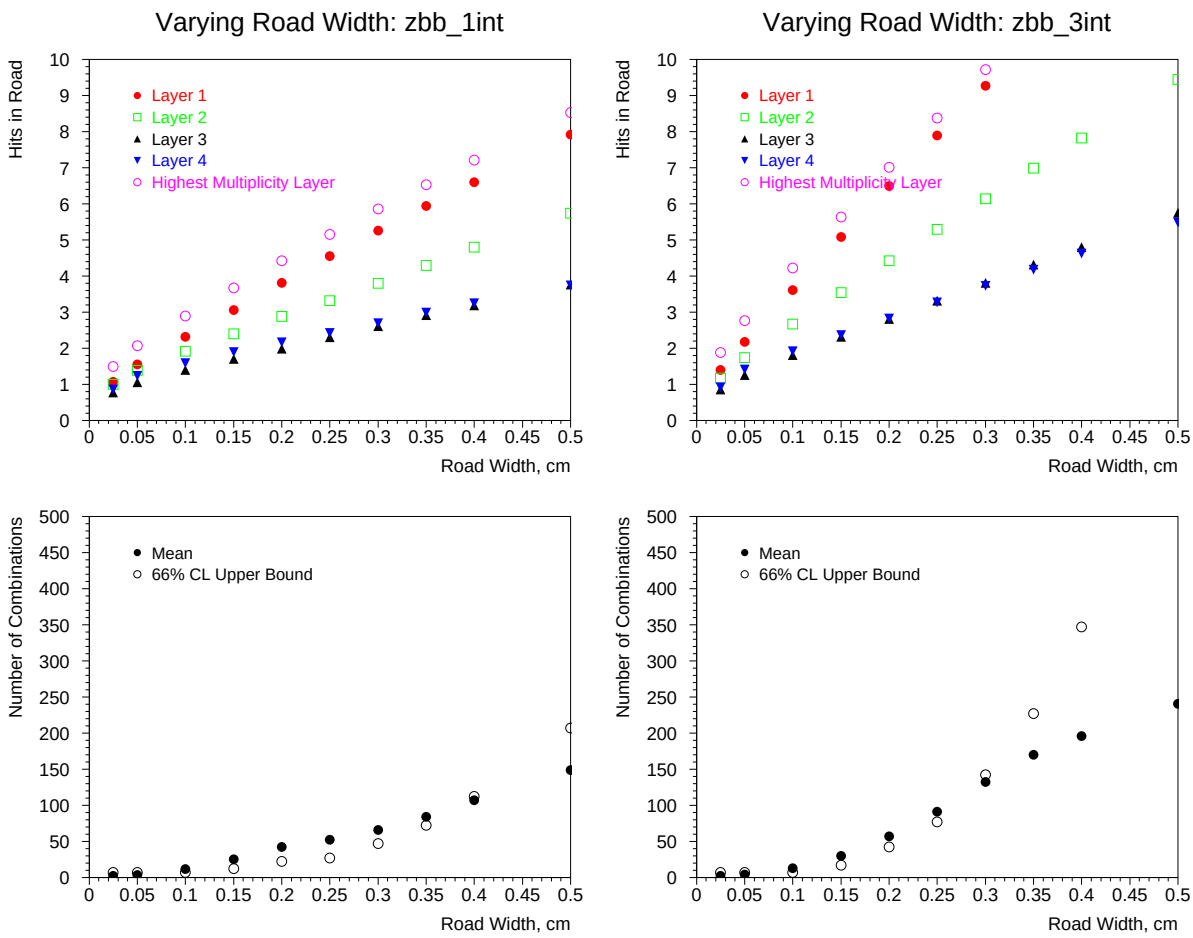

Figure 5: Hit multiplicity/layer/road and number of valid hit combinations/road for the $Z \to b\bar{b}$ samples as a function of road width. The standard road is ± 1 cm.

3.1 Physics Performance

We judge the performance of each algorithm using three figures of merit determined from Monte Carlo event samples:

1. **purity** defined as the fraction of reconstructed tracks having identically one Monte Carlo track contributing hits,

2. **efficiency** defined as the number of tracks which pass the requirement[5] $\chi^2/n < 3$ divided by the number of tracks with hits in three or more layers and

3. **trigger efficiency** for the dedicated L2STT triggers in the PAC '98 trigger menu[4].

The "good" track definition $\chi^2/n < 3$ was determined using the single muon sample with $p_T > 15$ GeV. Figure 6 shows χ^2/n for all tracks in this sample fitted using the static road/4 algorithm. Overlaid on this histogram is the expected shape of χ^2/n for three degrees of freedom. The histogram and expected shapes agree for $\chi^2/n < 3$, thus motivating the good track definition.

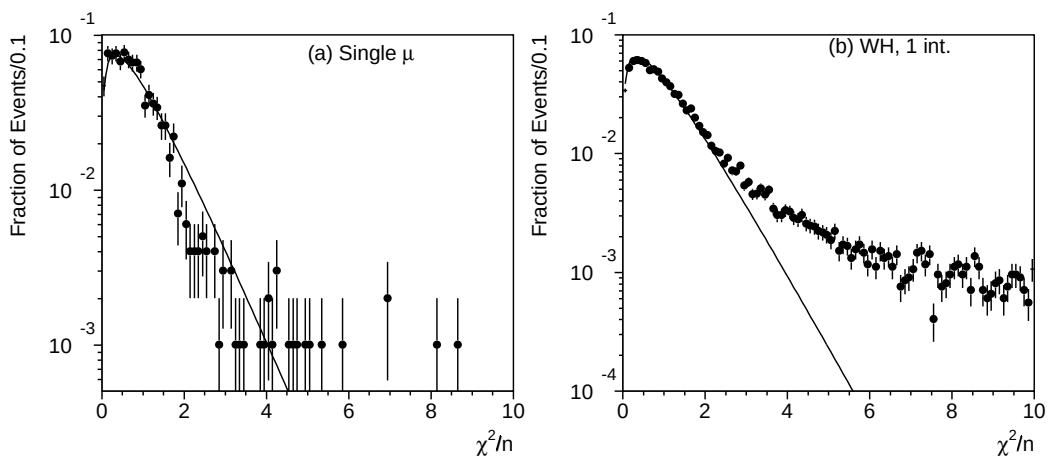

Figure 6: The χ^2/n distribution from the dynamic road/4 algorithm for tracks in (a) the 15 GeV single muon sample and (b) the $WH \rightarrow q\overline{q'}b\overline{b}$ (1 interaction) sample. The curve represents the expected χ^2/n for $n = 3$. The muon sample has limited statistics, but it clear that the fit χ^2 distribution begins to diverge from the expected distribution somewhere in the region $2 \leq \chi^2/n \leq 4$. The $WH \rightarrow q\overline{q'}b\overline{b}$ sample has significantly better statistics and shows a similar effect (although some of the χ^2/n tail must come from multiple scattering of low p_T tracks).

In practice, the good track definition will be tuned, and it will probably use a requirement on χ^2/n as a function of p_T. Figure 7 shows the purity versus efficiency for each sample and

[5] Here n is the number of degrees of freedom

Fit Algorithm/ Minimum Hit Layers	Single μ	$Z \to b\bar{b}$				$WH \to q\bar{q}'b\bar{b}$		QCD bkg.	
		1 int.		3 int.		1 int.		1-7 ints.	
		All	Good	All	Good	All	Good	All	Good
Static Road/4	1.0	0.43	0.87	0.19	0.84	0.49	0.88	0.31	0.84
Static Road/3	1.0	0.75	0.85	0.68	0.82	0.78	0.86	0.70	0.84
Dynamic Road/4	1.0	0.49	0.85	0.28	0.82	0.53	0.87	0.34	0.84
Dynamic Road/3	1.0	0.75	0.82	0.71	0.79	0.77	0.84	0.72	0.84
All Combinations/4	1.0	0.67	0.83	0.61	0.81	0.69	0.85	0.62	0.82
All Combinations/3	1.0	0.79	0.81	0.73	0.76	0.81	0.83	0.77	0.79
Best at layer/4	1.0	0.59	0.85	0.51	0.82	0.62	0.87	0.55	0.83

Table 2: Track purity for single tracks as defined in the text. Only events which pass level one triggers expected to feed to L2STT are used. Columns labelled "All" are for all tracks in such events. Columns labelled "Good" are for tracks which satisfy $\chi^2/n < 3$.

each fitting algorithm. Each point on a curve corresponds to the efficiency and purity for a specific χ^2/n in the range $1 \leq \chi^2/n \leq 100$. It is clear from this figure that the three–layer algorithms give higher absolute efficiency and for fixed efficiency tend to give better purity. From inspecting the distributions of $\chi^2(fitted\ parameters\ -\ true\ parameters)$ for tracks which fail $\chi^2/n < 3$ (hereafter called "bad" tracks), it is clear that the good track definition used here does not introduce a significant bias in one algorithm different from that in other algorithms.

Table 2 presents the single–track purities, and Tab. 3 gives the single–track efficiencies. The tables include all samples listed in Tab. 1 and events must pass the level one trigger conditions in PAC '98 which feed L2STT. Figures 11 through 50 show the distributions of the number of trial track fits/road, efficiency versus *true* particle p_T, efficiency versus *true* particle b, purity versus *true* particle p_T, purity versus *true* particle b (for all tracks and for good tracks only), fit χ^2/n versus *true* particle p_T, fit χ^2 versus *true* particle b, the χ^2 for the difference between the reconstructed track parameters and true track parameters versus *true* particle p_T, and the same quantity versus *true* particle b for each of the $Z \to b\bar{b}$ and $WH \to q\bar{q}'b\bar{b}$ samples.[6]

The overall trigger efficiencies are given in Tab. 4 to 7 with one table for each of the samples. The results relative to the trigger used in the PAC '98 studies are also shown in Fig. 8.

4 Timing Studies

A number of different processor options are being considered. The possibilities are (1) a DØ standard Compaq/Digital AXP-based board, (2) TI320C67 floating point DSPs, or (3) arrays of programmable logic devices.

[6] The QCD background sample shows similar results, but the statistical precision is considerably worse.

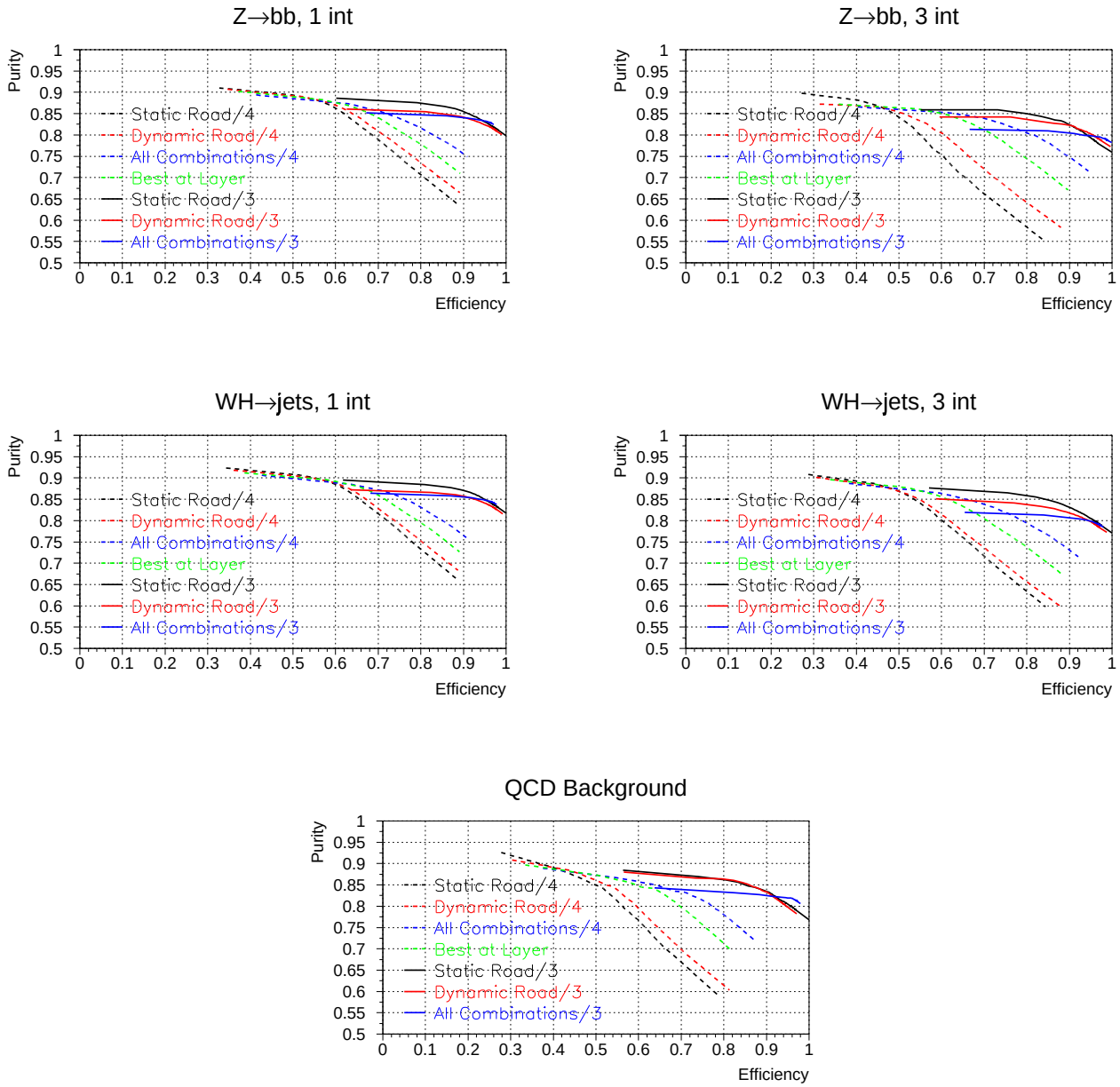

Figure 7: Purity vs. Efficiency for each of the data samples. The dotted lines are for the four–layers–required algorithms, and the solid lines are for the three–layers–allowed algorithms. For all samples the algorithms in order of lowest curve to highest curve are static road/4, dynamic road/4, best at layer, all combinations/4, all combinations/3, dynamic road/3 and static road/3. (At the highest efficiencies, the three–layer algorithms cross over each other.)

Fit Algorithm/ Minimum Hit Layers	Single μ		$Z \to b\bar{b}$ 1 int.		$Z \to b\bar{b}$ 3 int.		$WH \to q\bar{q'}b\bar{b}$ 1 int.		QCD bkg. 1-7 ints.	
	ϵ	ϵ_ρ	ϵ	ϵ_ρ	ϵ	ϵ_ρ	ϵ	ϵ_ρ	ϵ	ϵ_ρ
Static Road/4	0.95	1.00	0.63	1.00	0.54	1.00	0.66	1.00	0.60	1.00
Static Road/3	0.99	1.04	0.86	1.54	0.80	1.75	0.87	1.50	0.81	1.71
Dynamic Road/4	0.96	1.01	0.66	1.06	0.58	1.14	0.68	1.04	0.61	1.07
Dynamic Road/3	0.99	1.04	0.88	1.57	0.84	1.83	0.89	1.52	0.83	1.70
All Combinations/4	0.97	1.03	0.78	1.27	0.74	1.54	0.79	1.23	0.75	1.39
All Combinations/3	0.99	1.05	0.94	1.62	0.91	1.96	0.94	1.58	0.91	1.85
Best at layer/4	0.97	1.02	0.71	1.14	0.68	1.33	0.72	1.12	0.70	1.23

Table 3: Track efficiency for single tracks as defined in the text. Only events which pass level one triggers expected to feed to L2STT are used. The columns labelled "ϵ" are the efficiencies, defined as the number of good tracks divided by the number of three–layer tracks. The columns labelled "ϵ_ρ" are the relative efficiencies defined as the number of good tracks for the given algorithm divided by the number of good tracks for Static Road/4.

Trigger	Static Road 4 Layer	Static Road 3 Layer	Dynamic Road 4 Layer	Dynamic Road 3 Layer	All Combinations 4 Layer	All Combinations 3 Layer	Best at layer 4 Layer
JET_2_MED	0.20	0.89	0.22	1.38	0.51	1.60	0.32
JET_2_MINCFT3	0.26	0.96	0.27	1.50	0.59	1.68	0.36
JET_3_MED	0.27	0.98	0.27	1.47	0.56	1.53	0.31
JET_3_MET	0.34	0.98	0.34	1.43	0.60	1.49	0.37
$Z \to b\bar{b}$	0.95	1.01	0.86	1.00	0.97	1.02	0.93
$t\bar{t}$	0.93	1.01	0.84	0.99	0.97	1.01	0.94
$ZH \to \nu\bar{\nu}b\bar{b}$	0.94	1.01	0.84	1.00	0.97	1.04	0.92

Table 4: Relative trigger efficiency for the dijet background sample for the STT triggers in the PAC '98 trigger list for each of the filtering algorithms. The relative trigger efficiency is defined as the efficiency for a given algorithm divided by the efficiency for the algorithm used in the PAC '98 analyses.

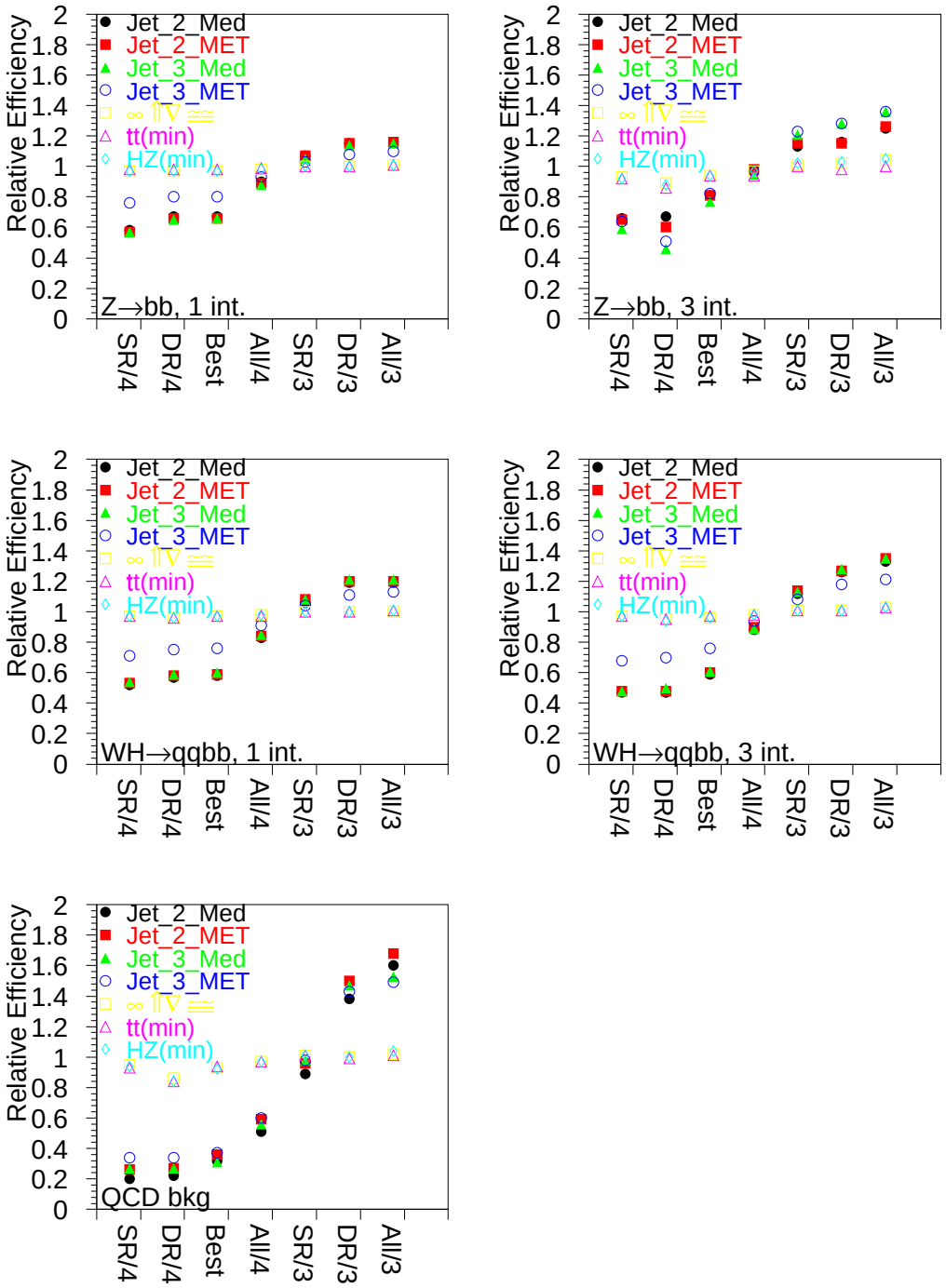

Figure 8: Relative trigger efficiencies for level two triggers in the PAC '98 studies which use STT information. Each panel is a different data sample, and the points give trigger efficiencies relative to the efficiency for the fitting algorithm used in the PAC '98 studies.

Trigger	Static Road		Dynamic Road		All Combinations		Best at layer
	4 Layer	3 Layer	4 Layer	3 Layer	4 Layer	3 Layer	4 Layer
JET_2_MED	0.58	1.07	0.67	1.15	0.90	1.16	0.67
JET_2_MINCFT3	0.57	1.07	0.66	1.15	0.89	1.16	0.66
JET_3_MED	0.57	1.05	0.65	1.14	0.88	1.15	0.66
JET_3_MET	0.76	1.03	0.80	1.08	0.93	1.10	0.80
$Z \to b\bar{b}$	0.97	1.00	0.97	1.00	0.98	1.01	0.97
$t\bar{t}$	0.98	1.00	0.98	1.00	0.99	1.01	0.98
$ZH \to \nu\bar{\nu}b\bar{b}$	0.97	1.00	0.97	1.00	0.98	1.01	0.97

Table 5: Relative trigger efficiency for the $Z \to b\bar{b}$(1 interaction) sample for the STT triggers in the PAC '98 trigger list for each of the filtering algorithms. The relative trigger efficiency is defined as the efficiency for a given algorithm divided by the efficiency for the algorithm used in the PAC '98 analyses.

Trigger	Static Road		Dynamic Road		All Combinations		Best at layer
	4 Layer	3 Layer	4 Layer	3 Layer	4 Layer	3 Layer	4 Layer
JET_2_MED	0.66	1.13	0.67	1.16	0.97	1.25	0.81
JET_2_MINCFT3	0.65	1.15	0.60	1.15	0.98	1.26	0.81
JET_3_MED	0.59	1.21	0.46	1.28	0.95	1.36	0.77
JET_3_MET	0.64	1.23	0.51	1.28	0.97	1.36	0.82
$Z \to b\bar{b}$	0.93	1.01	0.89	1.02	0.97	1.04	0.94
$t\bar{t}$	0.92	1.00	0.86	0.98	0.94	1.00	0.94
$ZH \to \nu\bar{\nu}b\bar{b}$	0.92	1.02	0.88	1.03	0.97	1.05	0.94

Table 6: Relative trigger efficiency for the $Z \to b\bar{b}$(3 interaction) sample for the STT triggers in the PAC '98 trigger list for each of the filtering algorithms. The relative trigger efficiency is defined as the efficiency for a given algorithm divided by the efficiency for the algorithm used in the PAC '98 analyses.

Trigger	Static Road		Dynamic Road		All Combinations		Best at layer
	4 Layer	3 Layer	4 Layer	3 Layer	4 Layer	3 Layer	4 Layer
JET_2_MED	0.52	1.06	0.57	1.19	0.83	1.19	0.58
JET_2_MINCFT3	0.53	1.08	0.58	1.20	0.84	1.20	0.59
JET_3_MED	0.54	1.08	0.59	1.21	0.85	1.21	0.60
JET_3_MET	0.71	1.04	0.75	1.11	0.91	1.13	0.76
$Z \to b\bar{b}$	0.97	1.00	0.96	1.00	0.98	1.00	0.97
$t\bar{t}$	0.97	1.00	0.96	1.00	0.97	1.01	0.97
$ZH \to \nu\bar{\nu}b\bar{b}$	0.97	1.00	0.96	1.00	0.98	1.01	0.97

Table 7: Relative trigger efficiency for the $WH \to q\bar{q}'b\bar{b}$ sample for the STT triggers in the PAC '98 trigger list for each of the filtering algorithms. The relative trigger efficiency is defined as the efficiency for a given algorithm divided by the efficiency for the algorithm used in the PAC '98 analyses.

4.1 AXP Processor

Some of the samples have been timed on a 500 MHz AXP processor. The results are given in Tab. 8. Fig. 9 shows the timing distributions for the $Z \to b\bar{b}$(3 interactions) sample for each of the fitting algorithms. The drastic effect of combinatorics producing tails is clearly seen.

Fit Algorithm/	$Z \to b\bar{b}$		$WH \to q\bar{q}'b\bar{b}$		QCD bkg.
Minimum Hit Layers	1 int.	3 int.	1 int.	3 int.	
Static Road/4	3.8	4.1	3.8	3.9	
Static Road/3	12.1	12.5	12.3	12.6	
Dynamic Road/4	7.1	8.2	7.0	8.2	
Dynamic Road/3	23.2	27.5	23.8	28.1	
All Combinations/4	16.7	18.7	16.2	19.9	
All Combinations/3	33.4	38.3	29.7	33.5	
Best at layer/4	10.5	11.2	10.6	11.8	

Table 8: Execution times/track (μs) for each algorithm on a 500 Mhz alpha processor.

4.2 Digital Signal Processors

Studies for a TI320C6x-based DSP solution indicate that a fixed-point DSP cannot provide the necessary performance because the floating point calculations needed to accomodate the dynamic range are emulated in a fixed point processor. Results from benchmarking "C"–level code using the TI tools for the C76 give the timing results shown in Tab. 9. The

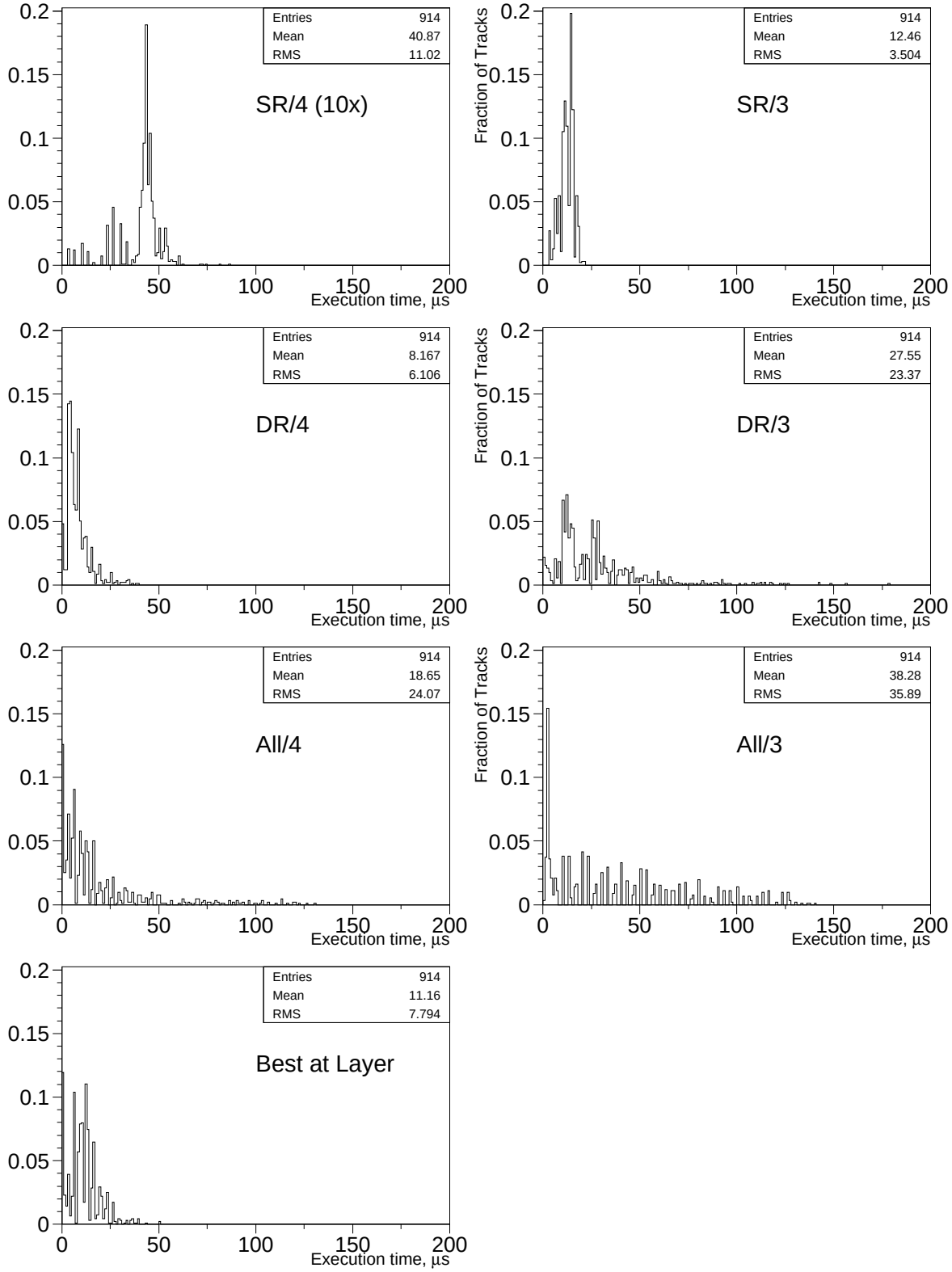

Figure 9: Fitting time per CTT road for each of the algorithms run on a 500 Mhz alpha processor.

time distributions are shown in 10 for approximately 250 tracks drawn from the $Z \to b\bar{b}$, 1 interaction sample.

Fit Algorithm/ Minimum Hit Layers	$Z \to b\bar{b}$ 1 int.	3 int.	$WH \to q\bar{q}'b\bar{b}$ 1 int.	QCD bkg.
Static Road/4	17±2			
Static Road/3	94			
Dynamic Road/4	46			
Dynamic Road/3				
All Combinations/4	332			
All Combinations/3				
Best at layer/4	88			

Table 9: Execution times/track (μs) for each algorithm on a TI C67 DSP with a 167 Mhz clock.

4.3 Programmable Logic

Finally, the static road algorithms have been implemented in an Altera 10k100KE programmable logic chip. Estimates based on first pass implementations of the static road/4 and static road/3 algorithms give 16 μs and 71 μs using the average hit/road multiplicity for the $Z \to b\bar{b}$ (1 interaction) sample.

5 Conclusions

The physics performance and processing times of seven different fitting algorithms have been studied using signal and background events. The physics performance studies indicate that it is important to allow reconstructed tracks to have only three of the possible four silicon layers used in the fit. The three–layer algorithms have track–by–track efficiencies 10-30% higher than the four–layer algorithms. Once three layers are allowed, the performance depends only slightly on the details of the hit selection. Because of this, the simplest of the three–layer algorithms, the "static road/3" algorithm will be used. This algorithm and the χ^2/n requirement defining good tracks may be further refined. For example, "static road/4" may be run, and only if the χ^2 is sufficiently poor, will the "static road/3" version be run.

Acknowledgements

We would like to thank Meena Narain who provided the $Z \to b\bar{b}$ samples, Dan Karmgard who pointed us to the single–μ sample and Jerry Blazey, Cecilia Gerber and Eric Smith for providing the QCD background data samples used here.

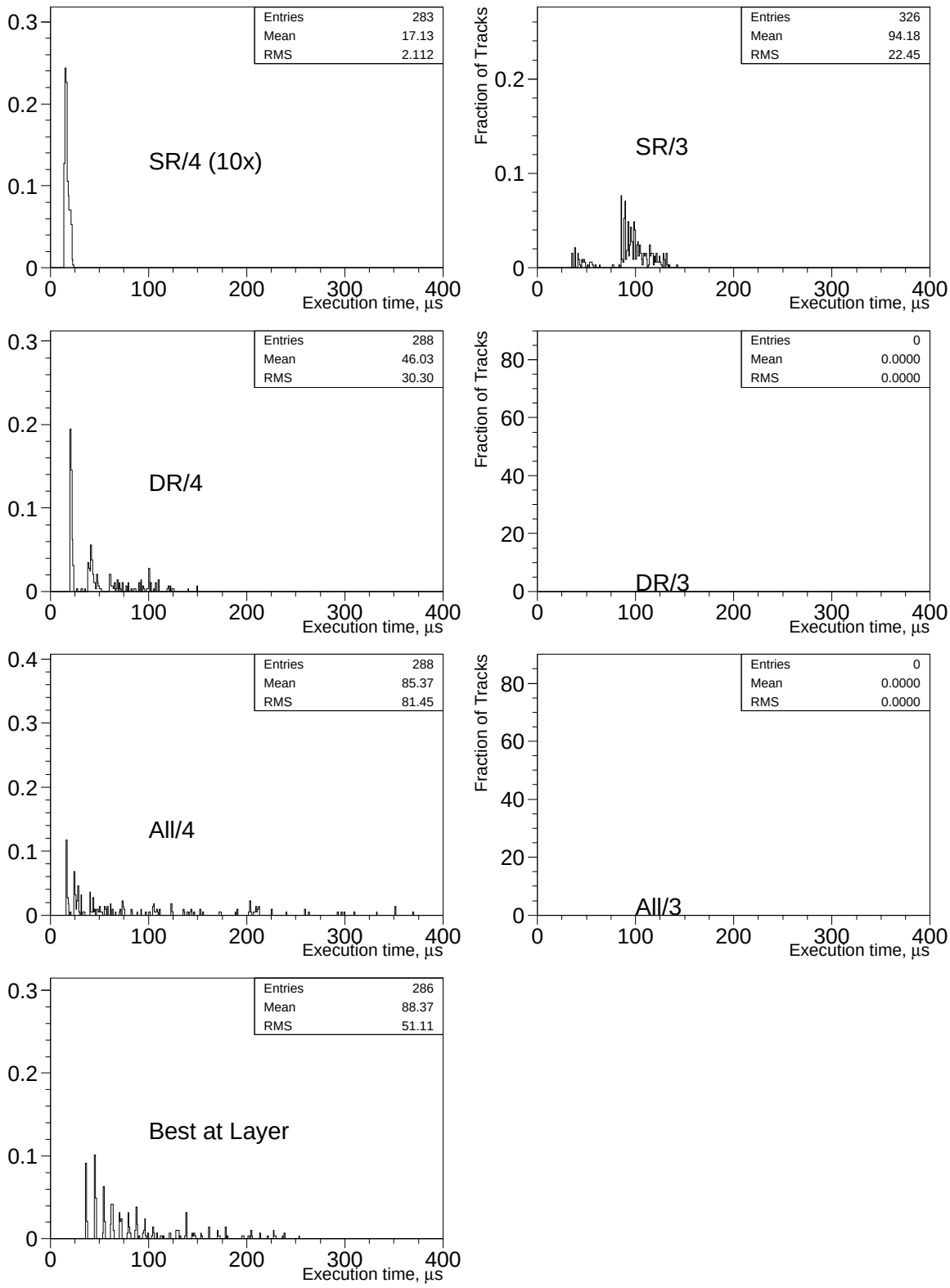

Figure 10: Fitting time per CTT road for each of the algorithms on a TI C67 DSP running at 167 Mhz.

References

[1] DØ Note 3363, *Road Definition for Silicon Track Trigger*, Uli Heintz

[2] See `http://www-d0.fnal.gov/~wahl/report/gut/d0n.ps`

[3] See `http://niuhep.physics.niu.edu/~blazey/run_ntuple_doc_v3.txt` The ntuples were regenerated to test the various fitting algorithms. However, the Monte Carlo files for the seven interaction samples in the p_T bins $10 \leq p_T \leq 20$ GeV, $20 \leq p_T \leq 40$ GeV, $40 \leq p_T \leq 80$ GeV and $80 \leq p_T \leq 500$ GeV are unavailable.

[4] DØ Note 3516, *A Silicon Track Trigger for the DØ Experiment in Run II*, and the additional information in `http://physics.bu.edu/~heintz/talk-pac99.pdf`

[5] See `http://www-d0.fnal.gov/~meena/d0_private/silicon/stt/dataflow_note.ps`